Stochastic Hydrology and Hydraulics 8, 57–77 © Springer-Verlag 1994

Modeling of transport in groundwater for environmental risk assessment

Y. Rubin and M. A. Cushey

Department of Civil Engineering, University of California, Berkeley, CA 94720, USA

A. Bellin

Department of Civil Engineering, University of Trento, Italy

Abstract: This paper presents the principles underlying a recently developed numerical technique for modeling transport in heterogeneous porous media. The method is then applied to derive the concentration mean and variance, the concentration CDF, exceedance probabilities and exposure time CDF, which are required by various regulatory agencies for risk and performance assessment calculations. The dependence of the various statistics on elapsed travel time, location in space, the dimension of the detection volume, natural variability and pore-scale dispersion is investigated and discussed.

Key words: Stochastic transport, risk assessment, concentration CDF, exceedance probabilities

1 Introduction

The increasing complexity of environmental regulations has made it necessary to formulate groundwater transport models in a probabilistic rather than deterministic framework. The appropriate type and form of model output is designated or implied by the applicable regulatory standard(s). For example, the U.S. Environmental Protection Agency (EPA) and the U.S. Nuclear Regulatory Commision (NRC) have promulgated regulations regarding the disposal of high level nuclear waste that stipulate specific exceedance probabilities and time oriented limits. The EPA rules include a containment requirement that the facility must be designed to assure that the probability of exceeding a radionuclide-specific cumulative release limit is less than 1 in 10 and the probability of exceeding ten times this limit is less than 1 in a 1000 over a 10,000 year period. In addition, the NRC rules include minimum groundwater travel times from the facility to the accessible environment.

An example of a regulation with an implied statistical approach is the requirement for a feasibility study to remediate a Superfund site under the Comprehensive Environmental Response, Compensation and Liability Act (CERCLA). These studies typically include a risk assessment which requires an exposure assessment aimed at quantifying the environmental fate and transport of contaminants to predict concentration levels over time at particular locations (Reichard et al., 1990; EPA, 1988). Transport modeling as part of the exposure assessment must provide input for other portions of the risk assessment and the estimated concentrations must be developed in a format consistent with the dose-response information (EPA, 1986a). For these instances, the type of output, its statistical moments, and the estimated time of exposure are important since the dose-response data may be in a variety of formats and can be for short or long time periods (Hallenback and Cunningham, 1986). In general, the risk assessment process encourages the use of stochastic formats to generate percentiles of concentration whenever possible (EPA, 1986b).

These regulatory trends are reflected in many recent studies involving contaminant transport modeling. Varshney et al. (1993) developed a framework for determining exceedance probabilities for analyzing the transport of pesticides in groundwater. Their results are presented as exceedance

probabilities versus pesticide concentration at a given time and location. McBean and Rovers (1992) analyzed the effect of assumed distributions on exceedance probabilities utilized as inputs to risk assessment. Helton (1993) developed a conceptual model to determine complementary cumulative distribution functions (CCDFs) to indicate the probability of exceeding individual consequence values as defined by the EPA release limits for high level nuclear waste repositories. Likewise, Cambell and Cranwell (1988) specify the need for results from flow and transport models to be in a probabilistic format to facilitate incorporation with other models to develop a CCDF of the released limits (or summed ratios) as part of a performance assessment for a proposed site. Dagan and-Nguyen (1989), Rautman and Treadway (1991) and Rubin and Dagan (1992) present their approach to account for geological uncertainties as part of an overall model to generate probability density functions (CDFs) of travel times for a nuclear waste repository to address NRC requirements.

Based on the present form of environmental regulations, it has become necessary to establish transport modeling techniques which can indicate the concentration and travel and exposure time of contaminants in a probabilistic format. The more appropriate forms of model output include exceedance probabilities over a range of concentrations and distribution functions for concentrations, mass releases, travel times and exposure times.

As already mentioned, an intensive research effort has been devoted in recent years toward modeling of contaminant transport in heterogeneous, geologically uncertain groundwater environments, and toward quantifying the associated uncertainties. No effort, however, was invested in developing a comprehensive yet computationally reasonable approach which is oriented toward regulatory-mandated risk and performance assessments. Specifically, there is a large disparity between the type and form of model output that is required by regulatory agencies for health and environmental risk assessment on one hand and the type of output that can be supplied by the most current methods. The reason is the enormous computational effort required to process and produce the necessary information. The statistics required are quite complex and computationally involved, yet the ability of the hydrologic community to stand up to the challenge is still limited. This leads to a growing difficulty in performance and risk assessment, and in turn to a slow response, cumbersome and sometimes belated decision-making process, and eventually to costly litigation.

The purpose of this paper is to review and assess some of the statistics required by the regulatory agencies for risk and performance assessment, and in particular on the effects of natural variability and geologic uncertainty. Our work is facilitated by capitalizing on a numerical method developed and presented in Bellin, Rubin and Rinaldo (1993) which is computationally very efficient. The numerical method is reviewed here briefly for completeness, and the larger part of this paper is devoted to new applications.

2 Methodology

The computations described in this paper were carried out using an algorithm which is described in Bellin et al. (1993). Since the description of the method is not the main goal of this paper, it is only briefly described in this section.

The basic idea of the algorithm is to achieve computational efficiency by relying on stochastic and geostatistical principles. We observe that:

1. The fluid velocity in heterogeneous media displays a seemingly random behavior. This randomlike behavior stems from the spatial variability of the hydraulic conductivity in the case of nonreactive transport, and in addition, from the variability of reaction coefficients when reactive transport is involved.
2. For a specified stochastic-spatial structure of the input hydrologic variables and for specified boundary conditions, the spatial correlation structure of the velocity can be derived using the flow equation (cf., Rubin, 1990, Rubin and Dagan, 1992, and Zhang and Neuman, 1992 for analytically-derived covariances based on assumption of small variability in the logconductivity, and Bellin et al., 1992, and Levin et al., 1992, for numerical solutions). The spatial correlation structure is expressed through a set of anisotropic covariances.
3. In the quite prevalent case of normally-distributed logconductivities (Hoeksema and K itanidis, 1984), and for relatively small logconductivity variance, the velocity is also Gaussian. In that case, its statistical structure is exhastively characterized through its expected value and spatial covariances.

4. The prediction of the velocity at a generic point $\mathbf{x}$ can be carried out using Gaussian conditioning (Mood and Graybill, 1963), which is mathematically analogous to kriging.

Consider that $\{N\}$ defines the N data available over the aquifer domain, i.e., measured data and coordinates. The estimator for the velocity $U(x)$ is given by $[\mathbf{U}(\mathbf{x})|\{N\}]$, with the vertical bar denoting conditioning. In practice, $[\mathbf{U}(\mathbf{x})|\{N\}]$ translates into a series of algebraic equations, which are well documented in the literature (Mood and Graybill, 1963; Journel and Huijbregts, 1978), and which require that the spatial covariances between the attributes contained in $\{N\}$ and U be known.

An important feature of the set $[\mathbf{U}(\mathbf{x})|\{N\}]$ is that it does not depend on actual values measured at the N nodes, but only on their relative spatial configuration. Additionally, among the N data available, the most influential will be those who are closest to $\mathbf{x}$. This effect is often referred to in the geostatistics literature as screening. The result is that the set $[\mathbf{U}(\mathbf{x})|\{N\}]$ can be replaced by $[\mathbf{U}(\mathbf{x})|\{N'\}]$, with N' representing only a portion of the N data which are nearest to $\mathbf{x}$, without any consequence to the actual results, but with a significant reduction in the computational effort.

The two properties of the set $[\mathbf{U}(\mathbf{x})|\{N\}]$ can be summarized succinctly in the following way:

- the set $[\mathbf{U}(\mathbf{x})|\{N\}]$ is equivalent to $[\mathbf{U}(\mathbf{x})|\{N'\}]$, with N' smaller than N, and with N' representing the measured data nearest to $\mathbf{x}$, under quite general conditions;
- the set of equations needed to solve for obtaining $[\mathbf{U}(\mathbf{x})|\{N\}]$ is equivalent to the set needed for solving $[\mathbf{U}(\mathbf{x}_1)|\{N_1\}]$, provided that $\{N\}$ and $\{N_1\}$ have the same spatial configuration, i.e., that $\{N\}$ and $\{N_1\}$ overlap if simply translated in space (and without rotation, if the spatial covariances are anisotropic).

At this point, the steps constituting the method employed here for transport calculations can be summarized as follows:

(i) Compute the spatial covariances of the velocity $\mathbf{U}$ for a given spatial structure of the logconductivity, Y, and for given boundary conditions and space dimensionality (this is just a preparatory step, and need not be carried out prior to any simulation if the applicable covariances are already available);

(ii) Define a set of nodes $\mathbf{x}_i$, i = 1, ..., M, which are spread over the aquifer domain. In our method, the set of nodes defines a regular grid. The goal is now to generate a large number of replicates of the velocity field. In each replicate, velocities are assigned to each of the M nodes, and it is understood that those velocities must be in agreement with the physics of the flow equation as well as spatially correlated as defined by the velocity covariances.

(iii) Compute the set of interpolation coefficients needed to project the relevant measurements in $\{N\}$ onto $\mathbf{U}(\mathbf{x})$. These interpolation coefficients are used to compute the conditional mean and conditional variance of $\mathbf{U}(\mathbf{x})$, conditional to $\{N'\}$, with $N' < N$.

(iv) Consider a generic node $\mathbf{x}_\ell$. Once the conditional mean and variance of $\mathbf{U}(\mathbf{x}_\ell)$ are available, they are used as input to a standard multivariate normal random generator, and random deviates are generated for the various components of the vector $\mathbf{U}$. The generated values are viewed as a realization of the velocity at node $\mathbf{x}_\ell$ for that particular realization.

(v) The velocity generated for node $\mathbf{x}_\ell$ is added to $\{N\}$, and we proceed now to a new node. We choose the next node such that we can condition its velocity on a subset of $\{N\}$ which is topologically identical to the one used at the previous node, such that there is no need to recompute the interpolation coefficients. Moving systematically over a regular grid, this is a very easy task to achieve, and the set $\{N'\}$ is taken as all the points within $\{N\}$ which fall within an a-priori defined search neighborhood.

(vi) Once velocities are computed over the set of M nodes, the production of a single replicate is completed. This procedure can be of course repeated as many times as needed, or according to some a-priori set convergence criteria. The set of coefficients, however, needs to be computed only once.

(vii) Transport is simulated over each replicate through particle tracking.

The generated velocity fields were shown (Bellin et al., 1993) to reconstruct the spatial structure as defined by the covariances. Furthermore, they are found to be mass conservative, within an acceptable error, which can be controlled by the spacing between the nodes.

The applicability of the methodology is restricted according to the assumptions employed in the derivation of the velocity covariances. For example, if the velocity covariances are derived under the assumption of small variability in the logconductivity, as is the case for all the analytically-derived velocity covariances presently reported in the literature, then the method in general is limited by that assumption.

The biggest advantage of the method, however, is in its computational efficiency. This advantage stems from the need to compute the set of interpolation coefficients only once, which it can then be used repeatedly for computing the velocity at each node. In other methods, notably the numerical ones, the production of each replicate requires solving the flow equation over the entire domain, and this effort needs to be repeated anew for each and every additional realization.

3 Visualization of the velocity field and of the plume

Figures 1 and 2 each depict a single realization of the generated velocity field, with each arrow representing the magnitude of the velocity and its direction. These figures were produced with the variances of the logconductivity σ_Y^2 equal to 0.2 and 0.8, respectively. The increase in σ_Y^2 clearly leads to a larger variability in the velocity field. While in the case of the small variance (Figure 1) the lateral components of the velocity are practically unnoticeable, these components become much more prevalent with an increase in the variance (Figure 2).

The variability in the velocity field metamorphoses continuously the topology of a solute body moving in that area. This has been demonstrated in several analyses of field studies. Modeling that process is a central issue in transport modeling, the difficulty arising mainly from the existence of sharp concentration fronts. One way to tackle that issue is to avoid it altogether, for example by representing the change in the geometry through the spatial moments of a cluster of particles which represents the plume (Smith and Schwartz, 1980; Bellin et al., 1992). The particle tracking technique assumes that the displacement of a solute parcel can be represented by the displacement of a material point of equivalent mass and which is located at its centroid. This assumption is of no consequence for computation of spatial moments. Difficulties arise, however, when there is a need to visualize the displacement of the plume, or whenever there is a need to compute concentrations. The reason is that a solute particle is not only being translated in space, it also changes its shape, and that effect cannot be modeled through the displacement of a material point. Furthermore, when it comes to measuring the concentration using a finite volume device, a material point can be modeled as either inside or outside the device, while in reality there is a large specrum of possibilities in between.

In order to enjoy the robustness of particle tracking on one hand, and preserve the integrity of the solute body on the other, we model its displacement in space through the translation of a cluster of particles which defines its circumference. Each point is translated independently of the others using fixed time steps, and the geometry of the solute body at each time step is computed by simply connecting all the points in the proper order. If pore scale dispersion is neglected, then the inside of this contour defines the area over which the concentration is equal to the initial one, C_0, while the outside is the area over which the concentration is naught. Concentration can assume values in between if the sampling device is covered only partly by the solute body.

The application of this method is demonstrated next. Figures 3 and 4 contain each a time sequence showing the evolution of a solute body whose initial geometry and position are depicted at $t = 0$, for σ_Y^2 equal to 0.2 and 0.8, respectively. Note that the mean flow direction is from left to right. In both cases, the edge of the solute body is jagged, and a larger distortion of the plume's original geometry occurs in the case of the larger variance. It also appears that the plumes are close to disintegrating into several smaller ones.

The effect of larger variances on spatial spread can be readily evaluated from these two figures. Figure 3 shows that the plume did not stretch laterally (normal to mean flow direction), while Figure 4 shows a considerable lateral stretching. The major impact, however, is manifested in the form of relative longitudinal (mean flow direction) displacement of the different portions of the plume. These observations are in agreement with theory (Dagan, 1984) which predicts larger longitudinal and lateral spreads with larger variances. It appears, however, that describing the shape of the plume through its moments is only partly informative, since in each realization the plume is not "space filling", but highly irregular.

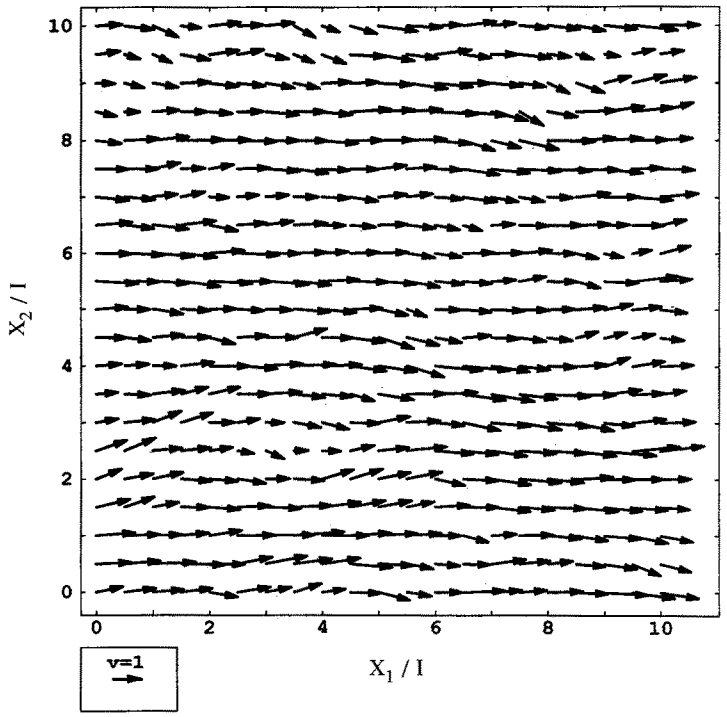

Figure 1. Example of a single replicate of the velocity field for $\sigma_Y^2 = 0.2$

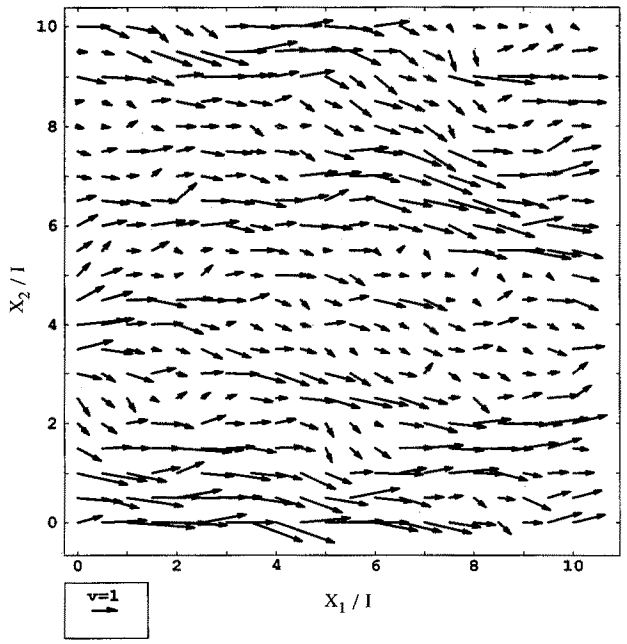

Figure 2. Example of a single replicate of the velocity field for $\sigma_Y^2 = 0.8$

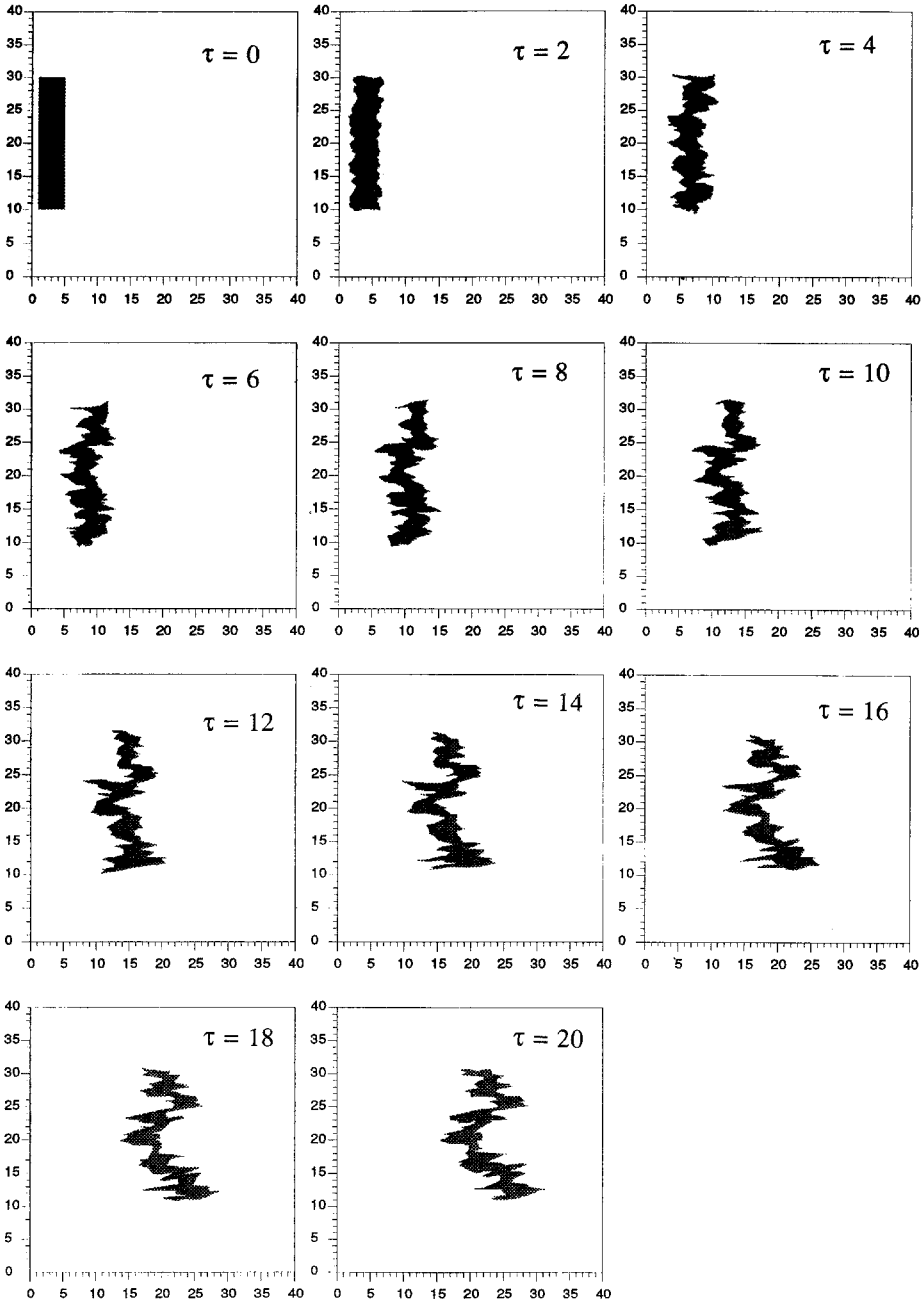

Figure 3. Example of the evolution of a solute body for $\sigma_Y^2 = 0.2$

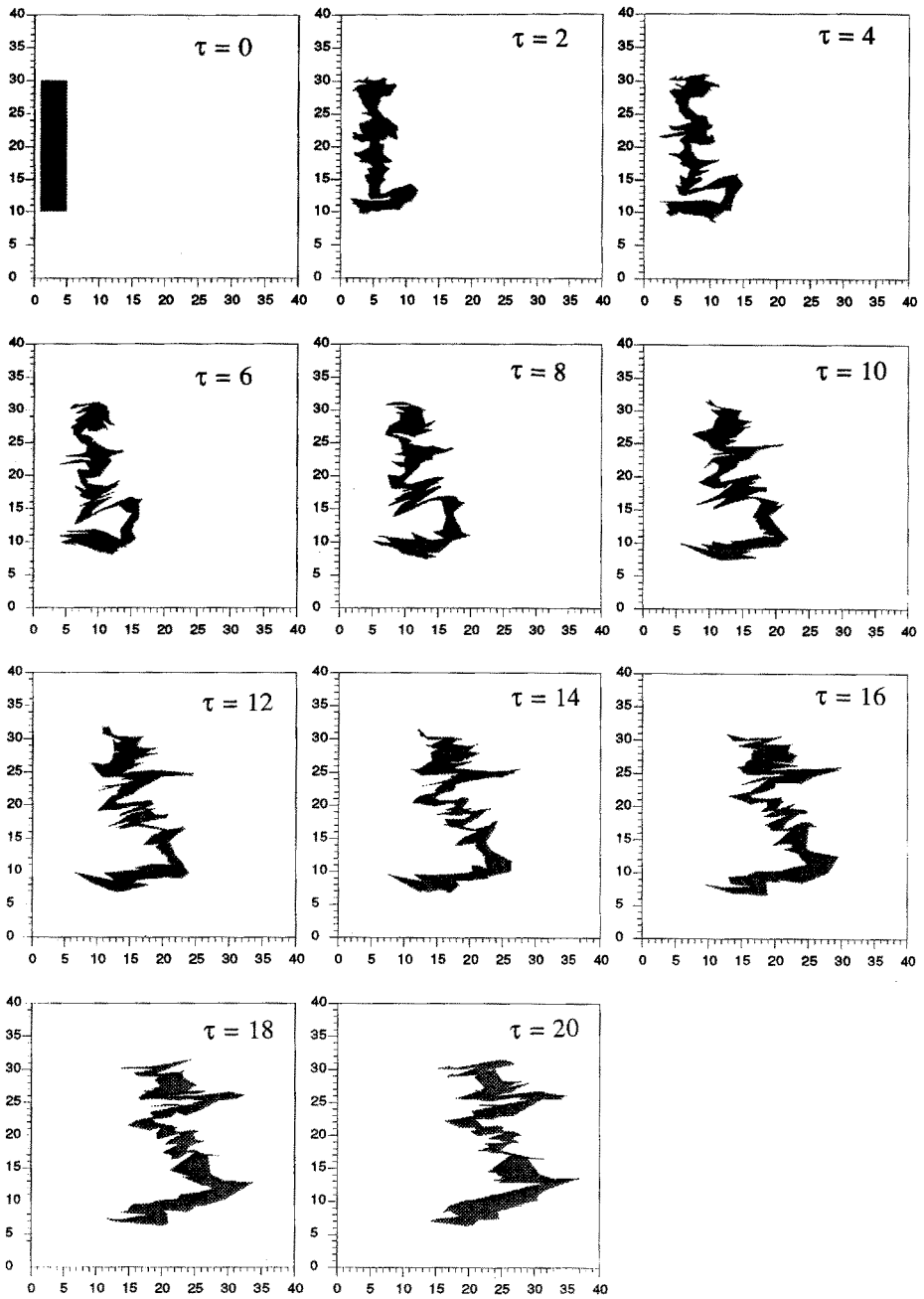

Figure 4. Example of the evolution of a solute body for $\sigma_Y^2 = 0.8$

4 On the concentration mean and variance

Different approaches for predicting solute concentrations in situations of natural heterogeneity and geological uncertainty were reported (Dagan, 1982; Graham and McLaughlin, 1989a, 1989b; Rubin, 1991a, 1991b; Vomvoris and Gelhar, 1990; Kabala and Sposito, 1992) and in general, they concentrate on the derivation of the first two moments of the concentration. Higher order moments can also be derived by some methods, but at an exorbitantly large computational price. This implies that in most approaches the concentration variance is viewed as the only means for quantifying uncertainty. The validity of this approach will be discussed subsequently, however, some analytical results for the first two moments of the concentration have been published, and are used here for validation purposes.

As an example, consider Figure 5, which depicts the geometry of an injection volume and that of a detection volume at a certain distance downstream. The mass injected is assumed to be spread uniformly over V_0, thus producing an initial concentration equal to C_0.

For application, we focus on the case of two-dimensional flow, uniform in the average, with the logconductivity Y being multinormal and defined by an exponential, isotropic covariance. The solution for the mean concentration is given by (Bellin et al., 1993):

$$\langle C(\mathbf{x},\tau)\rangle = \frac{\sqrt{X_{11}(t)\,X_{22}(t)}}{8\ell_1\ell_2\Delta_1\Delta_2}\sum_{i=1}^{4}\sum_{j=1}^{4}(-1)^{i+j}$$

$$\left\{Z_i\mathrm{erf}[Z_i] + \frac{1}{\sqrt{\pi}}\exp[-Z_i^2]\right\}\left\{W_j\mathrm{erf}[W_j] + \frac{1}{\sqrt{\pi}}\exp[-W_j^2]\right\} \qquad (1)$$

with

$$Z_1 = \frac{x_1 - x_{1,0} + \Delta_1/2 + \ell_1 - \tau}{\sqrt{2X_{11}(\tau)}};\quad Z_2 = \frac{x_1 - x_{1,0} + \Delta_1/2 - \ell_1 - \tau}{\sqrt{2X_{11}(\tau)}}$$

$$Z_3 = \frac{x_1 - x_{1,0} - \Delta_1/2 - \ell_1 - \tau}{\sqrt{2X_{11}(\tau)}};\quad Z_4 = \frac{x_1 - x_{1,0} - \Delta_1/2 + \ell_1 - \tau}{\sqrt{2X_{11}(\tau)}}$$

$$W_1 = \frac{x_2 - x_{2,0} + \Delta_2/2 + \ell_2}{\sqrt{2X_{22}(\tau)}};\quad W_2 = \frac{x_2 - x_{2,0} + \Delta_2/2 - \ell_2}{\sqrt{2X_{22}(\tau)}}$$

$$W_3 = \frac{x_2 - x_{2,0} - \Delta_2/2 - \ell_2}{\sqrt{2X_{22}(\tau)}};\quad W_4 = \frac{x_2 - x_{2,0} - \Delta_2/2 + \ell_2}{\sqrt{2X_{22}(\tau)}}$$

with notations defined on Figure 5. X_{11} and X_{22} are the longitudinal and lateral single particle displacement variances (Dagan, 1984). Figure 6 depicts the numerical results obtained for the case of a line source with $\ell_1 = 0.01I$ and $\ell_2 = 1I$ (I being the integral scale of the logconductivity) and for different times and for three detection volumes. The logconductivity variance σ_Y^2 was set at 0.2. The numerical results compare quite favorably with the analytic solution (equation 1).

Closed-form, analytic results for the concentration variance were reported in the literature by Vomvoris and Gelhar (1990) and Dagan (1982). In both cases the concentration is given for a "point" detection volume. Only Dagan (1982) reports a solution for the case of no pore scale dispersion, in the form:

$$\frac{\sigma_c^2(\mathbf{x},\tau)}{C_0^2} = \frac{\langle C(\mathbf{x},\tau)\rangle}{C_0}\left(1 - \frac{\langle C(\mathbf{x},\tau)\rangle}{C_0}\right) \qquad (2)$$

where σ_c^2 is the concentration variance, τ denotes time, and $C(\mathbf{x},\tau)$ denotes the concentration at $\mathbf{x}$ at time τ. Since pore scale dispersion and an increase in the dimension of the detection volume both act to reduce variability in the concentration, the concentration variance as given by equation 2 constitutes an upper bound.

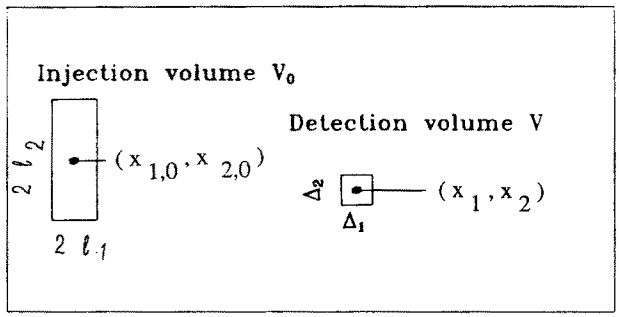

Figure 5. Example of injection and detection volumes, with nomenclature used in equation 1

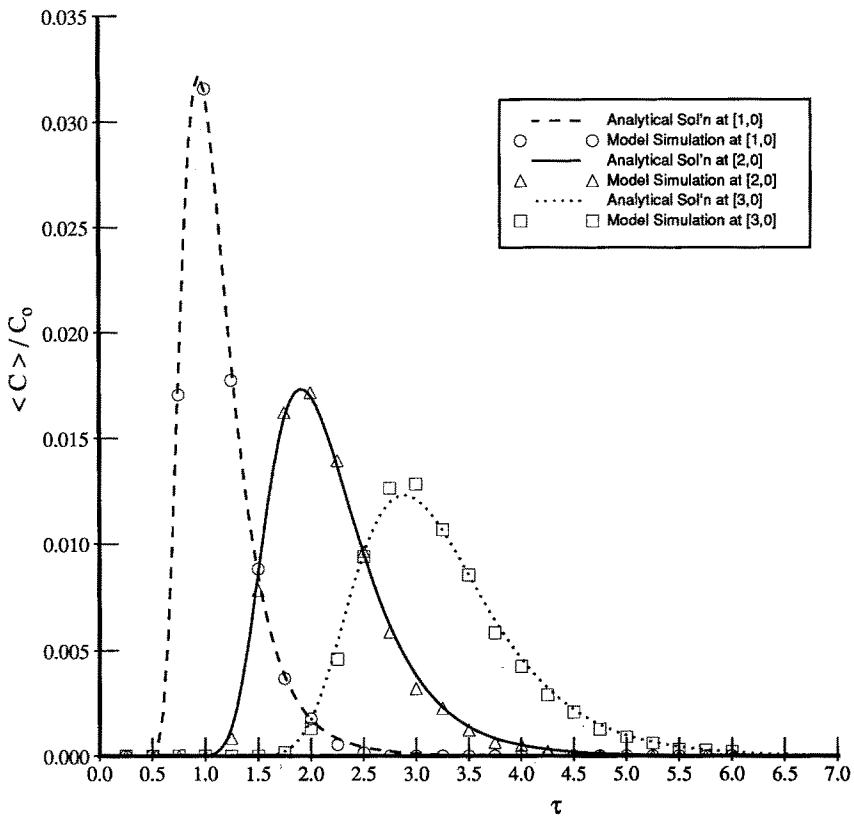

Figure 6. Comparison of analytical solutions for the mean concentration with model results at 3 locations for $\Delta = 0.1$ and $\sigma_Y^2 = 0.2$

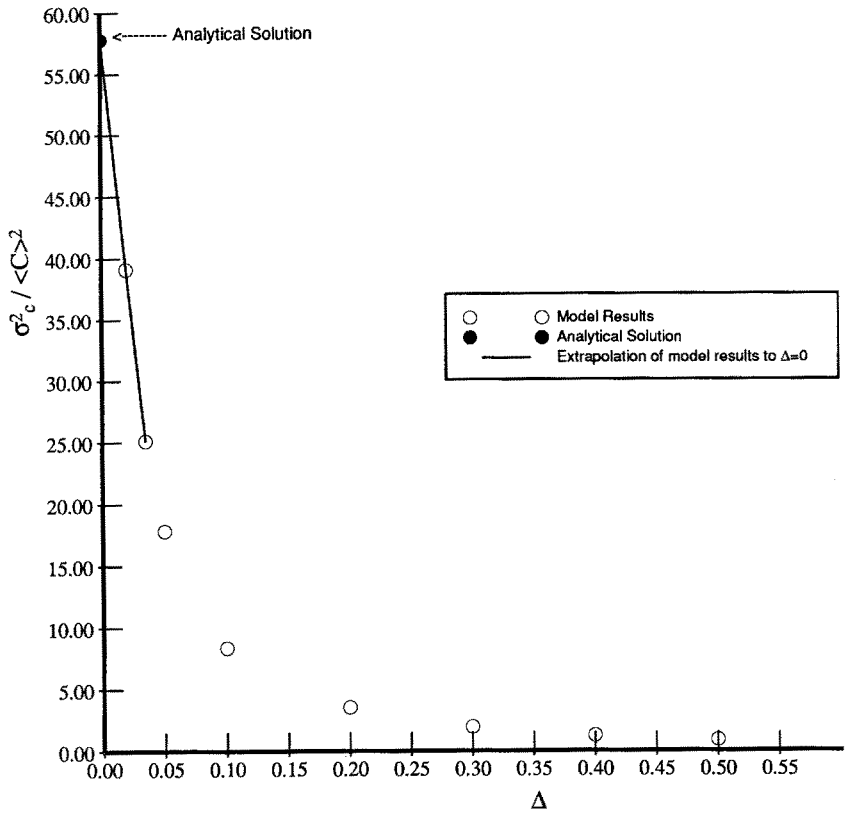

Figure 7. Comparison of the analytical solution for the coefficient of variation with model results extrapolated to $\Delta = 0$ for $\sigma_Y^2 = 0.2$, location [2,0],, and $\tau = 2$

Figure 7 depicts the concentration's coefficient of variation as a function of the dimension of the detection volume Δ. The detection volume is located two integral scale downstream from the source, x and all the other parameters are precisely those employed to produce Figure 6. As Δ decreases, the coefficient of variation increases. The intercept of the line connecting the two points nearest the origin falls exactly on the analytic result computed by equation 2, and this confirms that the asymptotic limit (equation 2) is in agreement with our results.

The results presented here and subsequently are applicable in a direct manner for the case of a non-reactive contaminant. However, simple transforms can be used in order to apply the results for the case of radionuclide transport since the displacement of the contaminant and the decay mechanism are independent of each other. For example, in the case of first-order decay, the mean concentration $\langle C(t) \rangle$ can be obtained by multiplying the present results by $\exp[-\lambda t]$ and the concentration variance can be obtained by multiplying the present results by $\exp[-2\lambda t]$, where λ is the radioactive decay constant.

5 The concentration's cumulative distribution function (CDF)

The use of the first two moments of the concentration for predictive purposes is justified when the concentration is either Gaussian or log-Gaussian. Bellin et al. (1993) showed that while for very large Δ, a Gaussian distribution, truncated at zero, can be used to model quite well the concentration, a general case for the concentration being either Gaussian or log-Gaussian cannot be made since the concentration is bounded by C_0 and zero. As a result, a fast way to compute the entire

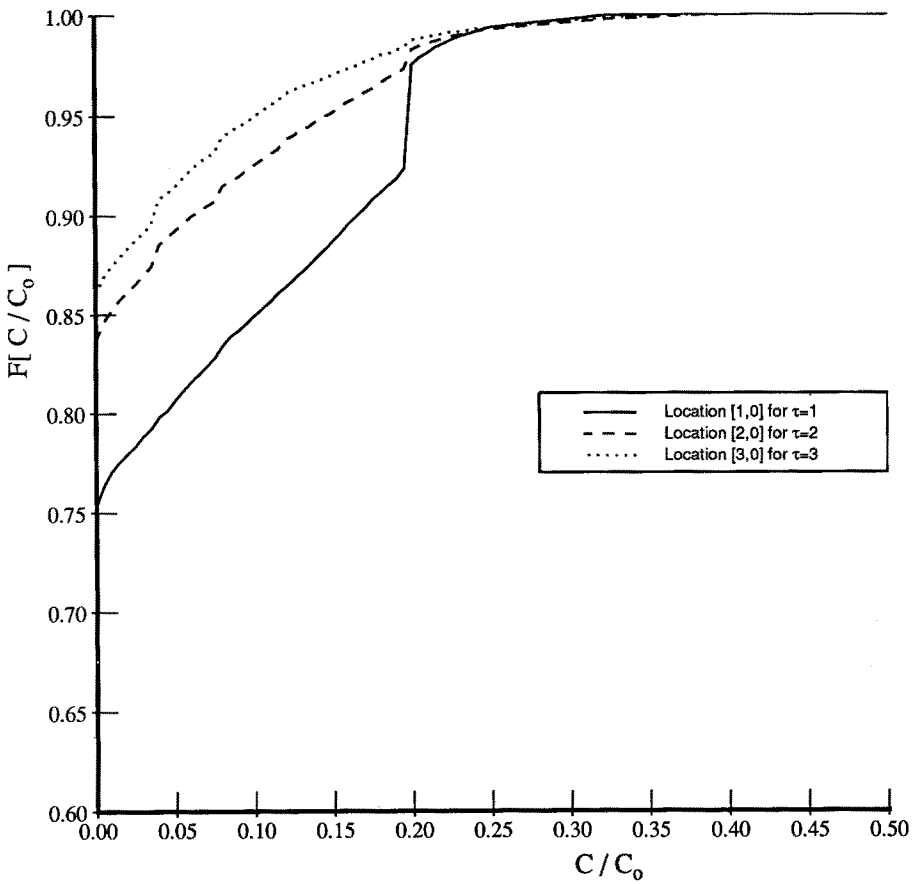

Figure 8. Cumulative probability distribution function of C/C_0 for different locations at mean travel times with $\Delta = 0.1$ and $\sigma_Y^2 = 0.2$ concentration's CDF, without assuming any parametric distribution,

appears to be a reasonable alternative.

Using our methodology, the concentration CDFs are easy to obtain, and are the subject of discussion of this section. Figure 8 depicts the concentration CDF at three different locations at times equal to the mean travel times to these locations.

The first thing to note about the shape of the CDFs is the large proportion of zero values, which increases with distance from the source. Another interesting point is the monotonous increase of the CDF from close to zero up to about $C/C_0 = 0.2$, followed by a discontinuity, which however becomes blurred with distance from the source. This is not a numerical artifact, but a physical effect. The value of 0.2 corresponds to the ratio between $2\ell_1$, the width of the initial volume, and Δ, the dimension of the detection volume. For a constant velocity field, the only two values possible for C/C_0 to assume are 0.2 and zero. In a heterogeneous field, this ratio can change if the plume changes it shape, i.e., becomes tortuous or disintegrates, such that particles that were originally side by side start to trail one another. The probability for that to occur near the source is small, since the shape of the plume is very much determined by its original shape. At larger times, however, the probability for such an occurrence increases, and the discontinuity will vanish altogether.

Figure 9 repeats the previous exercise, but using $\sigma_Y^2 = 0.8$. It shows that the proportion of zeroes increases, which is of course the result from the enhanced scatter of the plume. The CDF is also smoother next to $C/C_0 = 0.2$. The larger variance leads to a larger possibility for the solute particles to realign or for the plume to disintegrate, and creates a wider range of possible values for C/C_0.

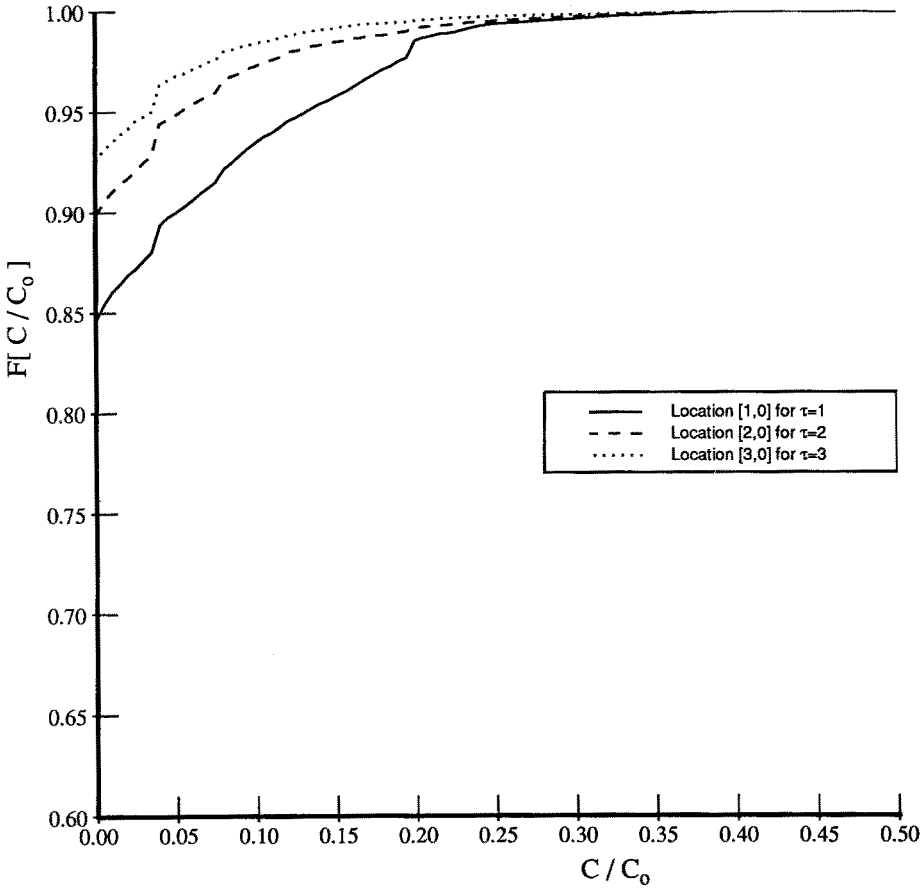

Figure 9. Cumulative probability distribution function of C/C_0 for different locations at mean travel times with $\Delta = 0.1$ and $\sigma_Y^2 = 0.8$

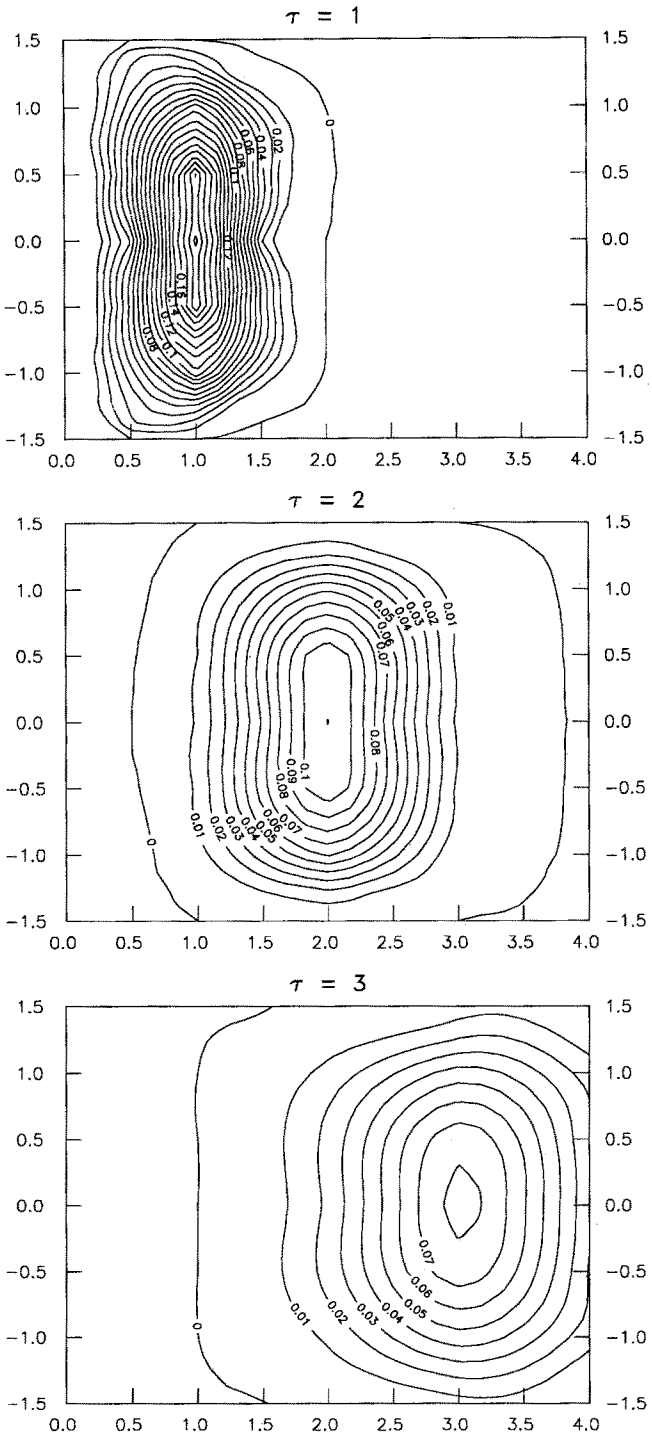

Figure 10. Exceedance probabilities for criterion C > 0.05 C_0 with $\Delta = 0.1$ and $\sigma_Y^2 = 0.2$ at (a) $\tau = 1$, (b) $\tau = 2$, and (c) $\tau = 3$ (coordinates in integral scale)

A statistic of importance from a regulatory point of view is the probability of the concentration exceeding an a-priori defined threshold value. Subsequently we refer to it as the exceedance probability. Figure 10 depicts a sequence of contour maps of the exceedance probability Prob[C $\geq$ 0.05 C_0] at nondimensional times τ = 1, 2, 3 (τ is defined as Ut/I, where U is the average velocity, t is dimensional time and I is the integral scale) with σ_Y^2 = 0.2 and for an initial injection volume as depicted on Figure 5 and for a detection volume of dimension 0.1I.

The shape and behavior of the "probability plume" resembles the behavior of a tracer plume: (i) the largest probabilities are located around the average travel distance (centroid) and it reduces with distance from the center; (ii) the plume's shape at small time is dictated largely by the shape of V_0, but much less so at larger τ, (iii) the exceedance probability reduces with travel time/distance, much like the maximum concentration itself.

Figure 11 shows a similar sequence, only for the case of σ_Y^2 = 0.8. The behavior of the "probability plume" is similar in principle to the previous case (Figure 10) only that the maximum exceedance probabilities are smaller. This can be explained by the larger spatial variability in the logconductivity which causes a larger spatial spread of the plume (cf., Dagan, 1984 for a theoretical derivation, Bellin et al., 1992 for numerical simulations) and this in turn reduces the probability to find a large number of solute parcels in any single detection volume. The reduction in the maximum exceedance probabilities around the centroid is accompanied by an increase in the exceedance probabilities away from the centroid. The larger σ_Y^2 leads to a larger spread in the velocity, and this implies that solute parcels can move either faster or slower than before, in both the mean flow direction and normal to it. Thus, solute parcels may appear now in places which were unreachable beforehand.

The resemblance between the probability plume and the concentration plume has been recognized in the past, but only indirectly. In the limiting case of an infinitely small detection volume and no pore scale dispersion, the concentration can be either zero or C_0. Its statistical distribution is bimodal, and given by (Dagan, 1982):

$$C = \begin{cases} C_0 & \text{Prob} = \frac{\langle C \rangle}{C_0} \\ 0 & \text{Prob} = 1 - \frac{\langle C \rangle}{C_0} \end{cases} \tag{3}$$

and hence it is completely determined by $\langle C \rangle$. Larger detection volumes alter the distribution from bimodal into a continuous one, but nevertheless, the underlying principle remains applicable. It can also be shown (Risken, 1984) that for Brownian motion, the concentration CDF satisfies the Focker Planck equation with velocities and dispersion coefficients identical to those which are used for the convection dispersion equation.

Rather than computing the concentration CDF at a single point, it can be computed over the entire domain. One way of representing the results is through a contour map of the different percentiles. Figure 12, for example, depicts the 95th percentile of C/C_0 with Δ = 0.1I at τ = 2 for σ_Y^2 equal to 0.2 and 0.8. The importance of this statistic is in signifying the probability of the extreme values in the distribution to be above the acceptable limits. We find higher values around the center in the case of the smaller variance, and lower ones away from the center. Note also that in the case of the smaller variance, the shape of the contours is dictated by the geometry of V_0, while an increase in the variance reduces that effect.

Another statistic of importance is the exposure time of the accessible environment to concentrations exceeding the acceptable limits. Its importance is in that it allows the computation of the source term for release of hazardous material to other pathways such as the atmosphere. Figure 13a depicts some generic results in the form of a CDF for the exposure time (non-dimensional) for concentrations above different critical values at a distance of two integral scales downstream from the injection point. The probability to observe a certain value of exposure time reduces as the critical value increases, and the proportion of zero exposure times increases. It is clear that as the threshold value increases, the CDF approaches a step function at τ_{exp} = 0.

The comparison in Figure 13b exposes the pattern of nonstationarity of the exposure time CDF. Translation along the mean flow direction leads to changes which are minor compared to those observed for translations normal to mean flow direction. Locations which are off the cen- troid's trajectory have a smaller probability for long duration exposures.

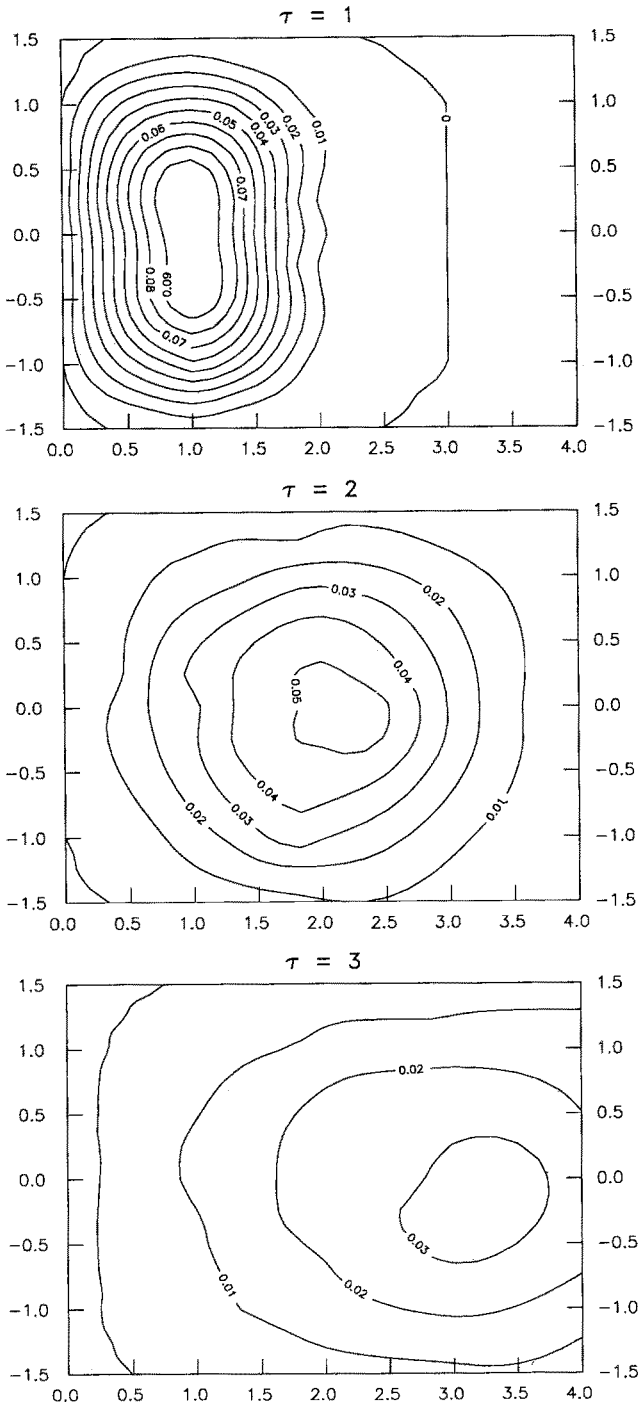

Figure 11. Exceedance probabilities for criterion $C > 0.05\ C_0$ with $\Delta = 0.1$ and $\sigma_Y^2 = 0.8$ at (a) $\tau = 1$, (b) $\tau = 2$, and (c) $\tau = 3$ (coordinates in integral scale)

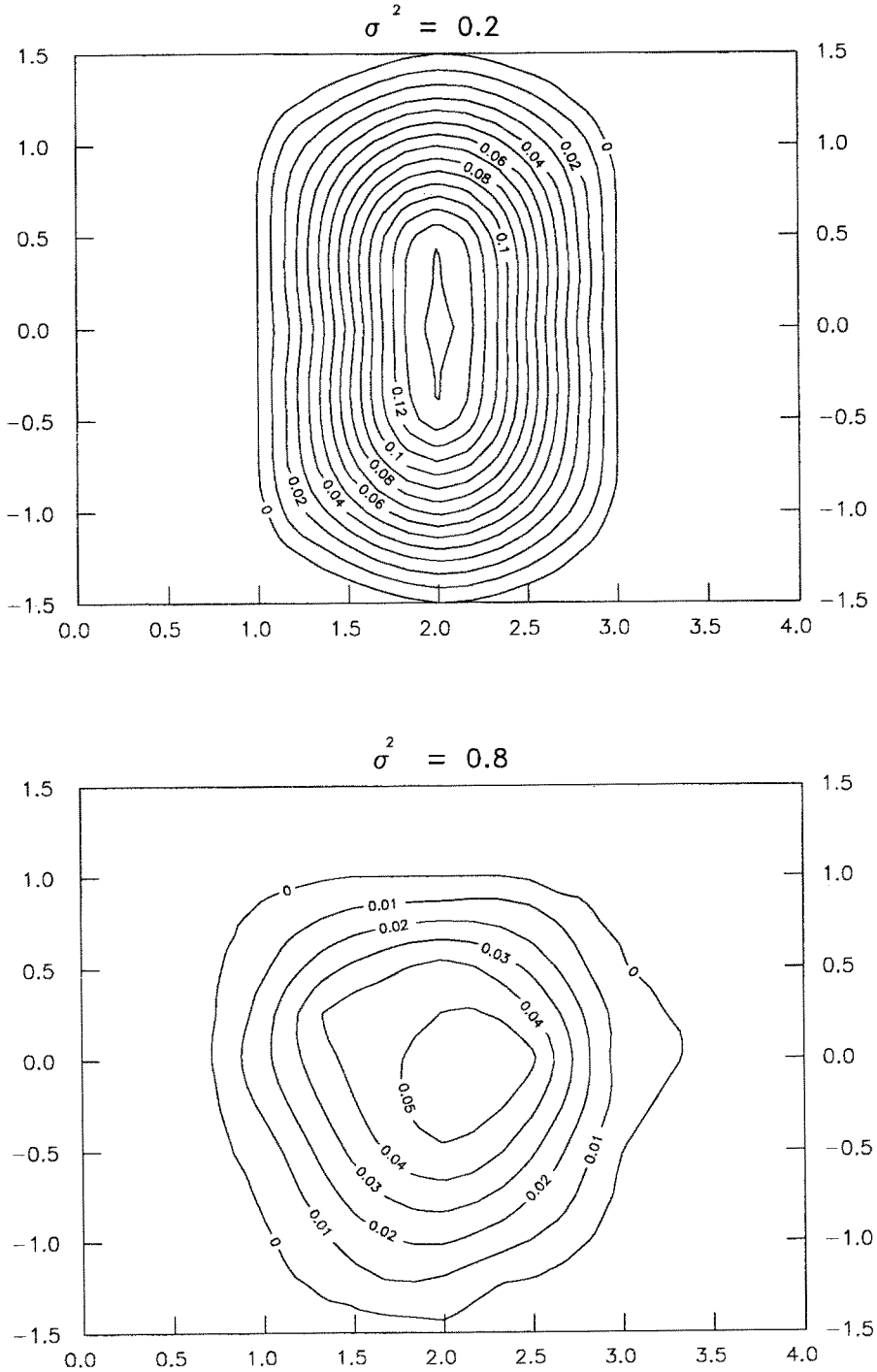

Figure 12. Ninety-fifth percentile of C/C_0 with $\Delta = 0.1$ at $\tau = 2$ for (a) $\sigma_Y^2 = 0.2$ and (b) $\sigma_Y^2 = 0.8$ (coordinates in integral scale)

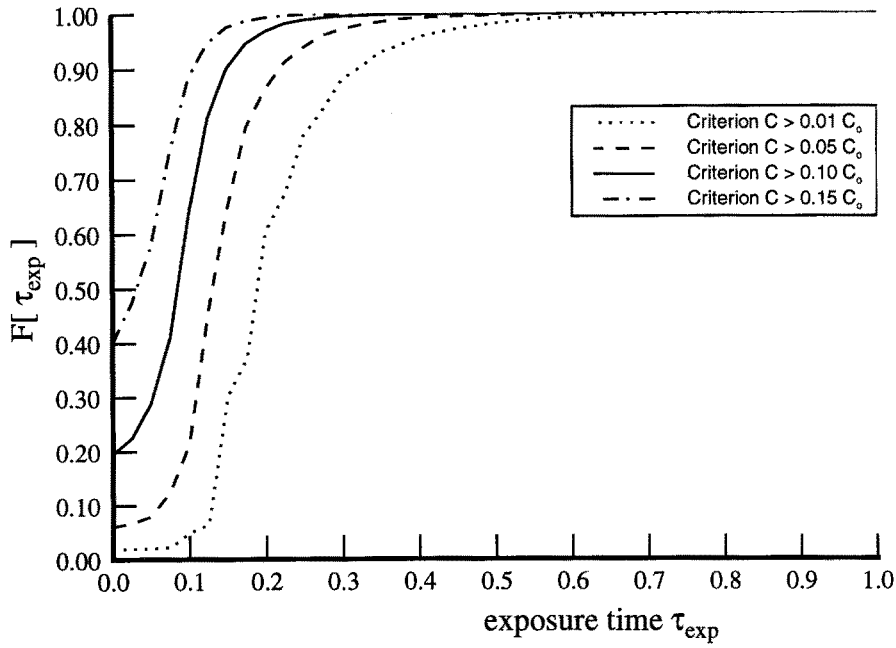

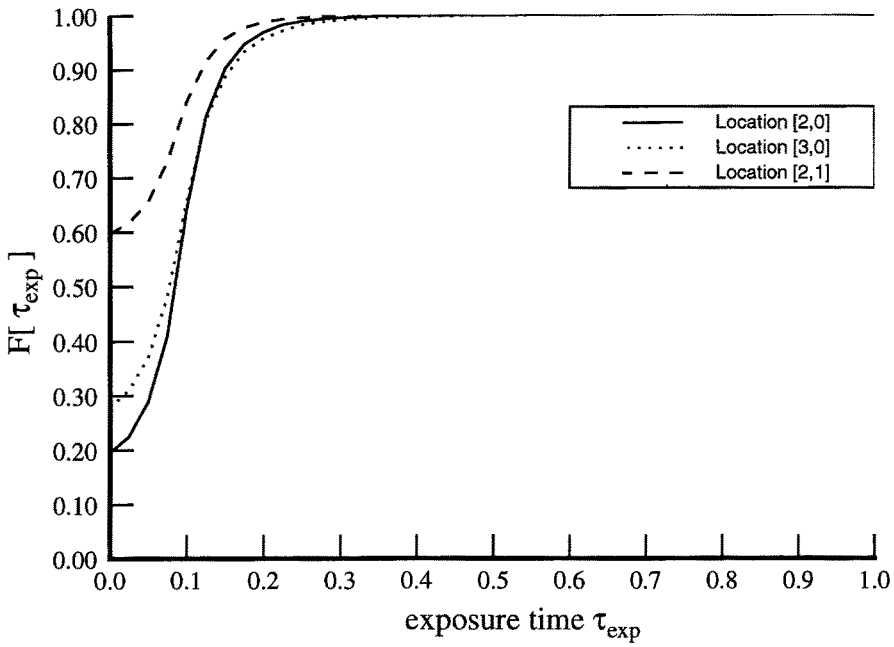

Figure 13. Cumulative distribution function of exposure time for (a) $\Delta = 0.1$ and $\sigma_Y^2 = 0.2$ at location [2,0] (b) criterion C > 0.1 C_0 with $\Delta = 0.1$ and $\sigma_Y^2 = 0.2$ at several locations

6 On the effects of pore-scale dispersion

Results discussed earlier in this paper were obtained for large Peclet number, i.e., under the assumption of negligible pore scale dispersion. In this section, the effect of pore scale dispersion (psd) is briefly discussed.

Consider first Figure 14. which shows the single particle displacement variances X_{11} and X_{22} for large Peclet number and for Peclet number equal to 10^2. We find that the effect of psd on the longitudinal displacement variance is quite small. It becomes more significant in the case of X_{22}, but for larger σ_Y^2 the effect of psd can be safely expected to become equally insignificant.

When dealing with the concentration CDF, however, the role of psd becomes much more significant. On Figure 15 we show the concentration CDF for large and small Peclet numbers, and for different Δ. In both cases, psd leads to a smaller variance by narrowing the range of observed values. The psd acts to dilute the mass contained in the solute parcels, and hence it reduces the maximum observed values on one hand, and it increases the proportion of non-zero values on the other. The increase in the non-zero values, however. does not prevent the shifting of the entire range of values toward smaller ones.

It appears also that psd is more significant for smaller Δ. For large Δ, a larger part of the displacements occurring because of psd leads to nothing but mass transfer within the detection volume boundaries, and hence the reduced effect.

7 Summary

This paper presents the principles underlying a recently developed numerical technique (Bellin et al., 1993) for modeling transport in heterogeneous media. The methodology developed based on these principles allows a significant reduction in the computational effort associated with deriving statistics which are necessary for environmental risk assessment.

The method is applied to derive the concentration mean and variance, the concentration CDF, exceedance probabilities and exposure time CDF. These statistics are required by various regulatory agencies.

We show that the concentration is generally non-Gaussian (Bellin et al., 1993, showed that a Gaussian model truncated at zero is applicable only for large detection volumes), and the availability of its first two moments is insufficient for predictive purposes. The concentration CDF strongly depends on location and on the elapsed time since injection. At early travel times, it also depends on the ratio between the dimension of the detection volume and injection volume, which determines an approximate upper bound on the concentration.

Larger variability in the logconductivity leads to a reduction in the probabilities to observe high concentrations in the area close to the plume's centroid, because of the enhanced spatial spreading of the injected mass. This, however, is associated with an increase in the probability to observe high concentration at locations away from the centroid.

Finally, the exposure time CDF is investigated, and is also found to be nonstationary, time dependent, with a smaller proportion of long exposure times as the variability of the medium increases.

Acknowledgement

This research was supported by NSF Grant EAR-9304481.

References

Bellin, A.; Rubin, Y.; Rinaldo, A. 1993: Eulerian-Lagrangian approach for modeling of flow in heterogeneous geological formations. Department of Civil Engineering, University of California at Berkeley. Report No. UCB/GT/93-05

Bellin, A.; Salandin, P.; Rinaldo, A. 1992: Simulation of dispersion in heterogeneous porous formations: statistics, first-order theories, convergence of computations. Water Resour. Res. 28(9), 2211-2227

Campbell, J.E.; Cranwell, R.M. 1988: Performance assessment of radioactive waste repositories. Science 239, 1389-1392

Dagan, G. 1982: Stochastic modeling of groundwater flow by unconditional and conditional probabilities, 2: The solute transport. Water Resour. Res. 18(4), 835-848

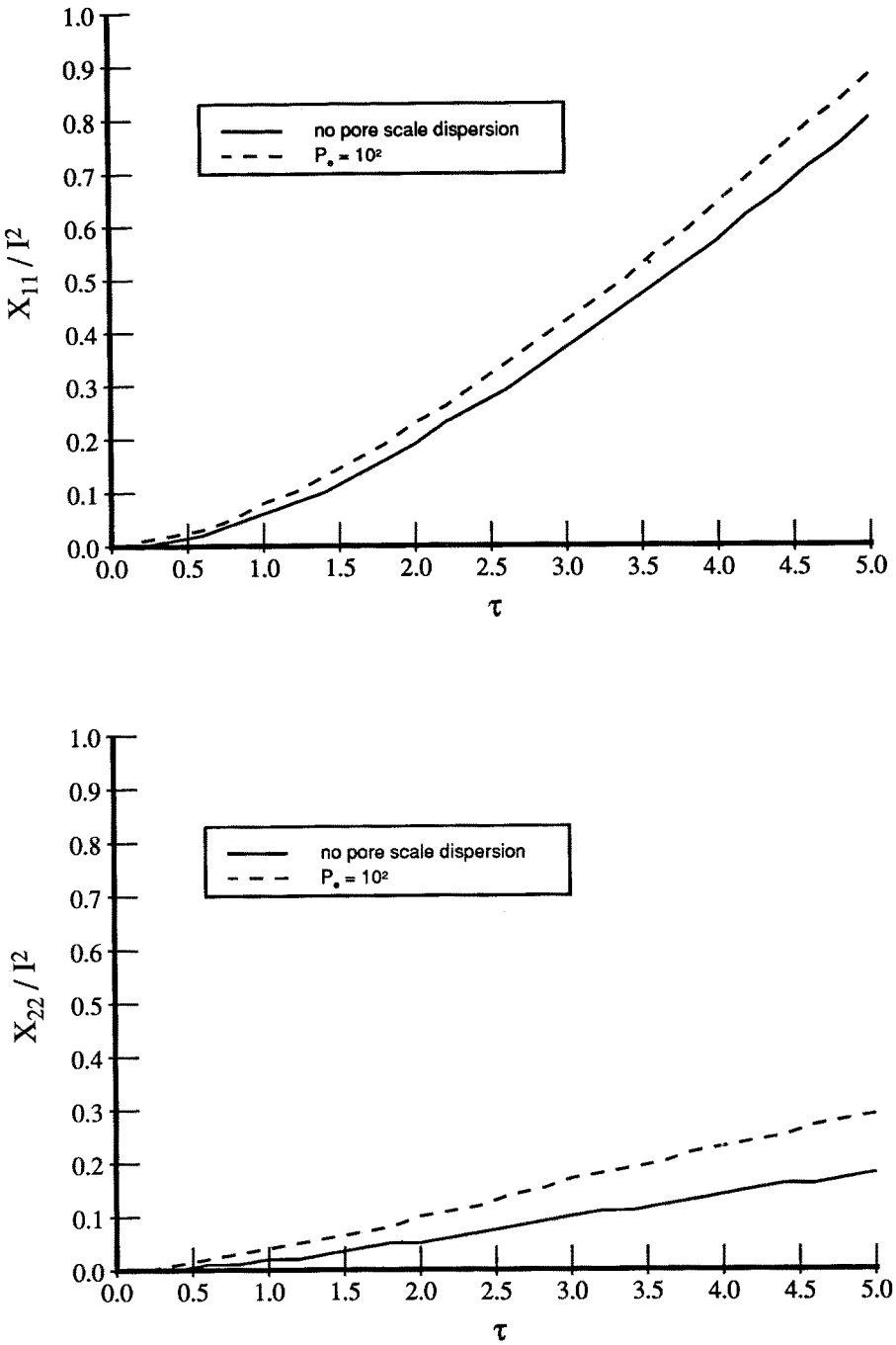

Figure 14. The effect of pore scale dispersion on the longitudinal and lateral single particle displacement variances (X_{11}/I^2 and X_{22}/I^2) for $\sigma_Y^2 = 0.2$

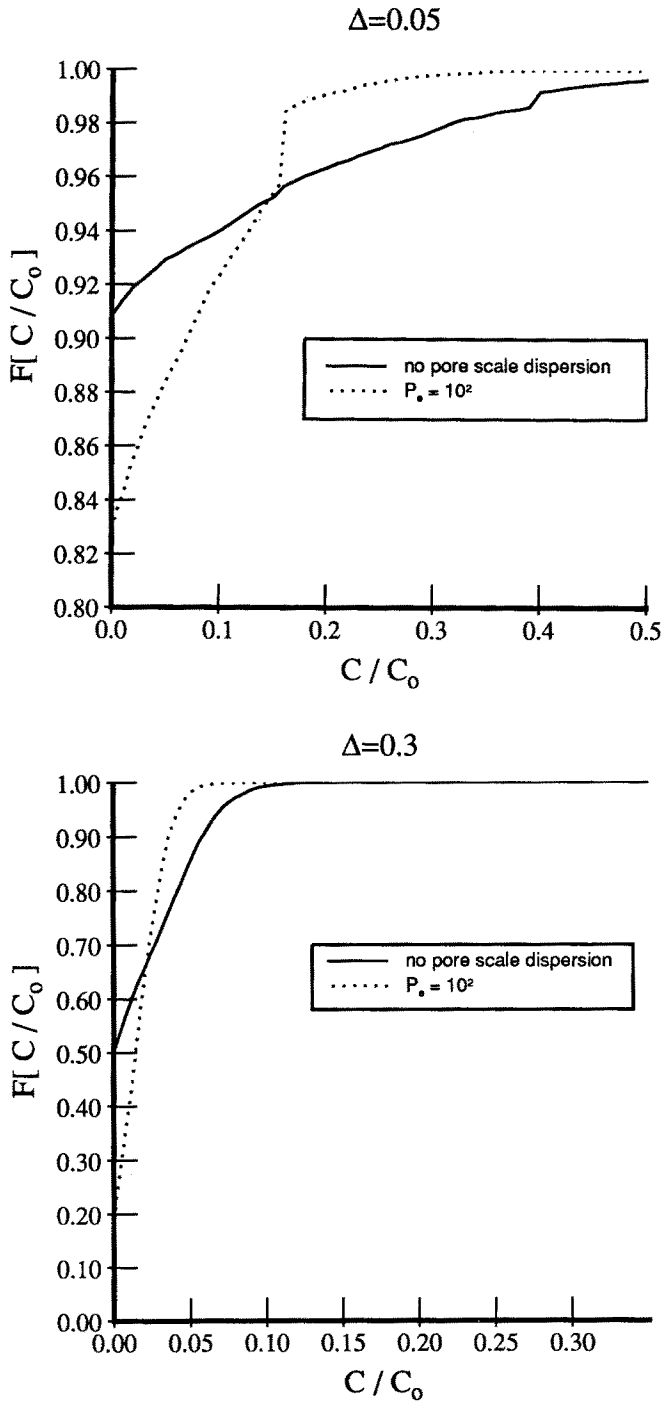

Figure 15. The effect of pore scale dispersion on the cumulative distribution function of C/C_0 for location [2,0] and $\sigma_Y^2 = 0.2$ at $\tau = 2$ for (a) $\Delta = 0.05$ and (b) $\Delta = 0.3$

Dagan, G. 1984: Solute transport in heterogeneous porous formations. J. Fluid Mech. 145, 151-177

Dagan, G.; Nguyen, V. 1989: A comparison of travel time concentration approaches to modeling transport by groundwater. J. Cantam. Hydrol. 4, 79-81

Environmental Protection Agency. 1986a: Guidelines for estimating exposures. Federal Register. 51(185), 34042-34054

Environmental Protection Agency. 1986b: Superfund Public Health Evaluation Manual. Washington, D.C. EPA/540/1-86/060

Environmental Protection Agency. 1988: Methods used in the United States for the assessment and management of health risk due to chemicals. Washington, D.C. EPA/600/D-89/070

Freeze, R.A. 1975: A stochastic-conceptual analysis of one-dimensional groundwater flow in nonuniform homogeneous media. Water Resour. Res. 11(5), 725-741

Graham, W.D.; McLaughlin, D. 1989a: Stochastic analysis of nonstationary subsurface solute transport, 1: Unconditional moments. Water Resour. Res. 25(2), 215-235

Graham, W.D.; McLaughlin, D. 1989b: Stochastic analysis of nonstationary subsurface solute transport, 2: Conditional moments. Water Resour. Res. 25(11), 2331-2335

Hallenback, W.H.; Cunningham, K.M. 1986: Quantitative risk assessment for environmental health and occupational health. Lewis Publishers, Inc. Chelsea, Michigan

Helton, J.C. 1993: Risk, uncertainty in risk, and the EPA release limits for radioactive waste disposal. Nuclear Tech. 101, 18-39

Hoeksema, R.J.; Kitanidis, P. K. 1984: An application of the geostastical approach to the inverse problem in two-dimensional groundwater modeling. Water Resour. Res. 20, 1009-1020

Journel, A.; Huijbregts, C. 1978: Mining geostatistics. Academic Press, London

Kabala, Z.J.; Sposito, G. 1991: A stochastic model of reactive solute transport with time-varying velocity in a heterogeneous aquifer. Water Resour. Res. 27(3), 341-351

Levin, O.; Zhang, D.; Neuman, S.P. 1992: Statistical properties of steady state 3-D Eulerian and Lagrangian velocity fields. Supplement to EOS. October 27, 1992

McBean, E.A.; Rovers, F. A. 1992: Estimation of the probability of exceedance of contaminant concentrations. Ground Water Mon. Rev. 12(1), 115-119

Mood, A.M.F.; Graybill, F. A. 1963: Introduction to the theory of statistics. 2nd ed. McGraw-Hill, New York

Rautman, C.A.; Treadway, A. H. 1991: Geological uncertainty in a regulatory environment; an example from the potential Yucca Mountain nuclear waste repository site. Environ. Geol. and Water Sci. 18, 171-184

Reichard, E.; Cranor, C.; Raucher, R.; Zapponi, G. 1990: Groundwater contamination risk assessment. International Association of Hydrological Sciences. Publication No. 196, Wallingford, UK

Risken, H. 1984: The Fockner-Planck equation. Springer-Verlag, Berlin

Rubin, Y. 1990: Stochastic modeling of macrodispersion in heterogeneous porous media. Water Resour. Res. 26(1), 133-141, and correction in Water Resour. Res. 26(10), 2631

Rubin, Y. 1991a: Prediction of tracer plume migration in disorder porous media by the method of conditional probabilities. Water Resour. Res. 27(6), 1291-1308

Rubin, Y. 1991b: Transport in heterogeneous porous media: Prediction and uncertainty. Water Resour. Res. 27(7), 1723-1738

Rubin, Y.; Dagan, G. 1992: Conditional estimation of solute travel time in heterogeneous formations: Impact of transmissivity measurements. Water Resour. Res. 28(4), 1033-1040

Smith, L.; Schwartz, F.W. 1980: Mass transport, 1: A stochastic analysis of macroscopic dispersion. Water Resour. Res. 16(2), 303-313

Varshney, P.; Tim, U.S.; Anderson, C. E. 1993: Risk-based evaluation of ground-water contamination by agricultural pesticides. Ground Water. 31, 356-362

Vomvoris, E.G.; Gelhar, L.W. 1990: Stochastic analysis of the concentration variability in a three-dimensional aquifer. Water Resour. Res. 26, 2591-2602

Zhang, D.; Neuman, S.P. 1992: Comment on "a note on head and velocity covariances in three-dimensional flow through heterogeneous anisotropic porous media by Y. Rubin and G. Dagan". Water Resour. Res. 28(12), 3343-3344